energy&fuels

pubs.acs.org/EF Article

Sunlight-Induced Molecular Progression of Oil into Oxidized Oil Soluble Species, Interfacial Material, and Dissolved Organic Matter

Phoebe Zito, David C. Podgorski, Tessa Bartges, François Guillemette, J. Alan Roebuck, Jr., Robert G. M. Spencer, Ryan P. Rodgers,* and Matthew A. Tarr*

Cite This: *Energy Fuels* 2020, 34, 4721−4726 Read Online

ACCESS | Metrics & More | Article Recommendations | Supporting Information

ABSTRACT: Spilled oil is highly susceptible to sunlight-induced transformations, both as films on the surface of water and material dissolved or dispersed in the water column. We utilized ultrahigh-resolution mass spectrometry and optical spectroscopy to understand shifts in oil photoproduct distributions as a function of photo-oxygenation. Oxygenation of oil produces compounds that have increased polarity, resulting in greater partitioning to the oil−water interface and eventually greater partitioning into the aqueous phase. Such partitioning was shown to be dependent on the carbon number and oxygen content of the photoproducts, providing an empirical basis for predicting the partitioning of oil photodegradation products between the oil phase, the interfacial region, and into the aqueous phase to form petroleum-derived dissolved organic matter. While such photochemical transformations have been predicted for many years, there has not been direct evidence previously for the photodissolution process. Furthermore, the relationship of carbon number and oxygen content with progression from the oil phase to the interfacial phase to the aqueous phase has not been demonstrated. This paper details this progression and observable properties that can be used to understand oil behavior after a spill during sunlight exposure, thus providing greater predictability of oil fate, transport, impact, and effective remediation strategies.

INTRODUCTION

Recent research has proven that sunlight initiates the formation of oxygenated species from petroleum.[1−6] Numerous papers have reported on the composition of these compounds in water through laboratory studies[7,8] and in field samples[4,9] in an effort to gain knowledge regarding their physical and chemical properties. However, none of these reports touched on the chemical progression that yields the introduction of these compounds into water. When oil undergoes abiotic or biotic processes, it becomes physically and chemically altered from the parent oil.[10] Once this chemical process occurs, newly oxygenated oil compounds are no longer oil soluble and begin to increase in water solubility. The process of becoming more water soluble depends on molecular size, structure, and the degree and nature of oxygenation. As the number of oxygen per molecule increases, the polarity increases, forming petroleum-derived dissolved organic matter or DOM_{HC}.[4,6]

The characterization of each fraction (oil, interfacial, and water) during the conversion of essentially water-insoluble petroleum molecules to DOM_{HC} has not previously been reported, and there is no existing evidence of the formation and transport of oxygenated petroleum compounds from the oil phase into water. While there have been several laboratory studies on thin oil film photodegradation in the presence of water,[7,11] the mechanisms to date have been unclear. Thingstad and Pengerud (1983) theorized that "photochemical oxidation of oil components leads to the formation of surface-active, oil-soluble compounds."[12] However, they did not provide definitive evidence that the "surface active" layer existed nor did they isolate or characterize all three of the layers involved in the progression of oil-soluble to interfacially active to water-soluble species.[12] This process can be described as a chemical transformation pathway of photodegraded petroleum compounds into more highly oxygenated species, which include photolabile (susceptible to light) and photorefractory (not susceptible to light) carbon. Although past studies reported on the weathering of petroleum and the formation of oxygenated, water-soluble petroleum compounds,[1,5,13−16] none has shown the existence of a progression mechanism that transfers these oxygenated compounds from oil to water (DOM_{HC}) via interfacial intermediates. The intermediate layer, interfacial material (IM), is a transitional layer of intermediate polarity that can be formed when oil is in contact with water, potentially creating a stable oil-in-water emulsion at the oil−water interface.[17] The IM layer is important to study because it impacts oil transport (increased viscosity), chemical character (increased oxygen content), and bioavailability (transition from IM to water-soluble species). Specifically, it plays a large role in emulsion formation and understanding the physical and chemical composition of the emulsion-stabilizing compounds in the IM fraction. This is an

Received: December 20, 2019
Revised: February 18, 2020
Published: February 21, 2020

https://dx.doi.org/10.1021/acs.energyfuels.9b04408
Energy Fuels 2020, 34, 4721−4726

important factor to consider when oil is in contact with water especially in refining[18,19] and when an aquatic oil spill occurs.

Complex mixtures require the use of a wide variety of advanced analytical techniques such as 3D-fluorescence and ultrahigh-resolution mass spectrometry in order to succeed in their characterization. Excitation emission matrix spectroscopy (EEMs) is a quick, highly sensitive, 3D fluorescence technique used to characterize complex mixtures and provide important insights into the composition of fluorophores in a sample. Ultrahigh-resolution mass spectrometry has the ability to assign elemental formulas to a wide range of the compounds present in complex mixtures. Specifically, Fourier transform ion cyclotron resonance mass spectrometry (FT-ICR MS) is used to understand compositional molecular level changes to complex mixtures after they are weathered or heavily processed.[20−22] The main objectives for this study were to (i) characterize the progression of oxygenated petroleum compounds moving from oil to IM and water under simulated sunlight conditions and (ii) provide optical data and elemental formulae to show changes in composition occurring in each fraction. These objectives help us understand an important mechanism driving the fate of oil spilled in aquatic systems (or refining) that will improve our knowledge of oil fate based on mass spectrometric and fluorometric measures. The importance of this fraction lies in its contribution to emulsion formation and stability. Its chemical polarity (induced by light) directly determines the formation of the soluble fraction (DOM_{HC}), which is crucial for understanding interfacial activity. To the best of our knowledge, this is the first reported study on the composition and role of the IM fraction after photo-oxidation.

MATERIALS AND METHODS

Samples and Reagents. Surrogate Macondo oil was provided by BP (August 2011, chain of custody number 20110803-Tarr-072). Seawater collected from the Gulf of Mexico by the Louisiana Universities Marine Consortium (35 g/kg, pH 8.3) was previously filtered through combusted (450 °C) 0.27 μm glass microfiber filters (Advantec) and irradiated prior to use in experiments for 12 h to decrease dissolved organic carbon (DOC) concentration (final [DOC] = 1.5 ppm) and any terrestrial signatures. All glassware was acid cleaned and combusted at 500 °C prior to use. Toluene, high-performance liquid chromatography (HPLC)-grade dichloromethane (DCM), heptane, and pentane were all purchased from VWR. For isolation and analysis of IM, HPLC-grade DCM, methanol (MeOH), *n*-heptane, toluene, and water were obtained from J.T. Baker (Phillipsburg, NJ). The pH ∼11 water was prepared by dropwise addition of Sigma-Aldrich (St. Louis, MO) ammonium hydroxide solution (28% in water). Chromatographic-grade silica gel (Fisher Scientific, 100−200 mesh, type 60 Å) was dried overnight in an oven at ∼110 °C.

Sample Preparation. Thin oil films (120 μm)[23] created with 325 mg of light oil were spread over 50 mL of preirradiated seawater. The oil films were exposed to simulated sunlight using an Atlas Suntest CPS solar simulator for 24 h (equivalent to 6 days of natural sunlight)[24] in 250 mL jacketed beakers thermostatically controlled at 27 °C. Exposures were performed in triplicate with a single dark control. The oil was removed from the surface of the water with a glass rod. The IM was isolated from the dark and oxidized oil following the methods reported by Jarvis et al.[25] and Clingenpeel et al.[17] The yield of the IM fraction was 24 wt % (77 mg) of the starting material (325 mg). The oil and IM were blanketed with argon gas and stored at 4 °C in the dark until analysis. DOM_{HC} was collected by separating the water from each oil after exposure. Water samples were subsequently filtered through 0.27 μm glass-fiber filters and stored under the same conditions as oil and IM.

Excitation-Emission Matrix Spectroscopy. Oil, IM, and DOM_{HC} samples were analyzed using excitation-emission matrix spectroscopy measured on a Horiba Aqualog. Refer to Supporting Information for instrument parameters, specifications, and blank EEM spectra for seawater (Figure S1).

DOC Measurements. DOC analysis used the high temperature catalytic/combustion oxidation method incorporating a Shimadzu TOC Analyzer and a platinized alumina catalyst. The acidified samples (pH 2) were sparged for 5 min at 75 mL/min with ultra-pure air to remove inorganic carbon from samples prior to measurement. The mean of three to five injections of 25 μL is reported for every sample. Precision, described as a coefficient of variance, was <2% for the replicate injections.

Mass Spectrometry. DOM_{HC} was collected and preconcentrated by the solid-phase extraction technique described by Dittmar et al. (2008).[26] Briefly, each sample was passed through a precombusted 0.27 μm glass-fiber filter and acidified to pH 2 prior to loading onto a Bond Elut PPL (Agilent Technologies) stationary phase cartridge. Previous studies report extraction efficiencies of DOM_{HC} at an average of 80 wt % when eluted from the PPL cartridge using methanol.[27] Each sample was then desalted with pH 2 Milli-Q water and eluted with methanol at a final concentration of 100 μg C mL^{-1}. Oil and IM samples were prepared in concentrations of 250 μg mL^{-1} in 1:1 toluene/methanol and 1% methanolic NH_4OH. The extracts, along with the oil and IM samples, were stored in the dark at 4 °C in precombusted glass vials until analysis by negative-ion electrospray ionization coupled with a custom-built Fourier transform ion cyclotron resonance mass spectrometer (FT-ICR MS) equipped with a 9.4 T superconducting magnet (National High Magnetic Field Laboratory (NHMFL), Florida State University, Tallahassee).[28,29] Negative mode electrospray ionization highlights the most acidic compounds in each fraction, as photo-oxidation yields abundant carboxylic acid-containing transformation products and other oxygenated compounds that can be ionized under the same electrospray conditions. Each mass spectrum was internally calibrated with a "walking" calibration equation with internally developed software provided by the NHMFL (Predator) followed by a molecular formula assignment by PetroOrg.[30,31] The structural features of these oxygenated compounds were refined based on classifications in a modified aromaticity index (AI), which provides definitive criteria for assignment of aromatic compounds detected in complex mixtures.[32] Using AI and elemental ratios of molecular formulas (H/C and O/C), the molecules can be classified according to stoichiometry.[32] Refer to Supporting Information for mass calibration and data analysis specifications.

RESULTS AND DISCUSSION

FT-ICR Mass Spectrometry Reveals a Molecular Progression. *Heteroatom Oxygen Class Graphs.* FT-ICR mass spectrometry exposes the molecular level progression of oxygenated compounds through comparison of the elemental compositions of the oil soluble, IM, and DOM_{HC} after photoirradiation. A comparison of the phototransformation products is provided in Figure 1, which summarizes the heteroatom oxygen class graphs for the FT-ICR MS data obtained in the triplicate analysis of the oil (black), IM (red), and DOM_{HC} (blue) fractions after simulated sunlight exposure. For each fraction, the graph presents the relative abundance of detected molecular formulae as a function of oxygen content from 1 to 18 oxygens per molecule with their associated relative abundance error. These data provide clear evidence that a molecular progression exists in photo-oxidized oil through the presence of pseudo Gaussian shifts to higher oxygen content as the compounds become less oil soluble and consequently partition away from the oil and into the IM and DOM_{HC} fractions. From the data shown in Figure 1, the

https://dx.doi.org/10.1021/acs.energyfuels.9b04408
Energy Fuels 2020, 34, 4721−4726

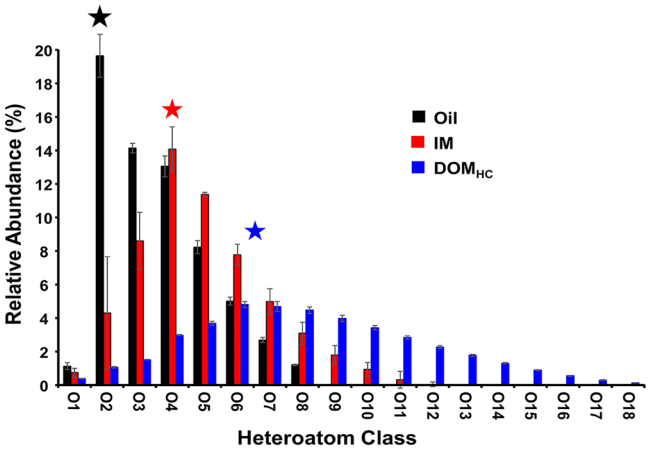

Figure 1. Heteroatom oxygen class graphs for the FT-ICR MS data obtained in the triplicate analysis of oil (black), IM (red), and DOM_{HC} (blue) fractions after simulated sunlight exposure.

following observations were made that increase our understanding of the oil photo-oxygenation process.

(1) Species that remained oil soluble contained 1−8 oxygens per molecule, with the most abundant species in the O_2 class (highlighted with a black star).
(2) Species that contained 1−12 oxygens were interfacially active and thus had an increased tendency to bind water, yet they remained associated with oil.
(3) The most abundant interfacially active species contained four oxygens per molecule (highlighted with a red star).
(4) The most water soluble species (DOM_{HC}) had the widest oxygen range and were composed of species that contained between 1 and 18 oxygens per molecule, with the most abundant DOM_{HC} species comprising between 6 and 7 oxygens per molecule (highlighted with a blue star).

Thus, the progression from oil- to water-soluble species contains an intermediate step (IM) that remains oil-associated but interfacially active. Evidence for interfacial activity is based on selective recovery of the IM.[17,25] Subsequent photo-oxidation of these photogenerated surfactants (IM) yields water-soluble species.

van Krevelen Diagrams Highlight Molecular Formulae of Each Fraction. Another way to visualize the data is through van Krevelen (vK) diagrams, which highlight global shifts in H/C versus O/C ratios for all assigned O_x species. Each dot on the graphs represents molecular formula of the same O/C and H/C ratios assigned from the mass spectral data.[22] Figure 2 is composed of the vK diagrams of the molecular formulae of each fraction and reveals the progression of higher oxygenated species from the oil to IM, and finally the produced DOM_{HC} (refer to Figures S2 and S4 for dark control). For the oil, the species have a narrow distribution of O/C ratios, predominantly less than 0.3, with the most abundant species at an O/C ratio of 0.1 (highlighted by red arrow). The IM material has a broader distribution of O/C ratios, including a shift in the most abundant O/C ratio and an increase in the most abundant species to an O/C ratio of 0.2. The change in the distribution is more pronounced for the DOM_{HC}, with the highest observed O/C ratios approaching 1, the most abundant O/C ratio ∼0.5, and the characteristic DOM "star pattern" centered at H/C = 1 (highlighted by black arrow) and O/C = 0.5. The vK diagrams shown in Figure 2

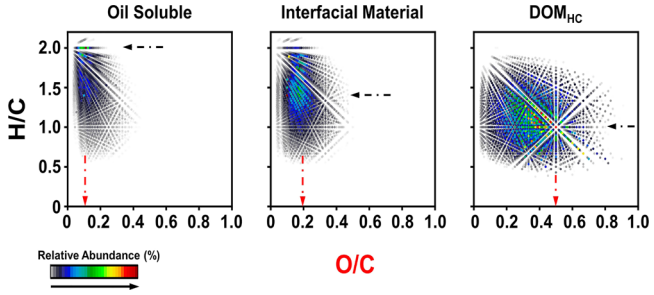

Figure 2. vK diagrams of the molecular formulae unique to each fraction shows the progression of higher oxygenated species from oil, IM, and DOM_{HC} fractions after simulated sunlight exposure. For each sample, black and red arrows highlight the most abundantH/C and O/C values, respectively.

also begin to shed light on the significant O_x heteroatom class overlaps highlighted previously in Figure 1, as the progression to a higher O/C ratio (red arrows) contains a concurrent progression to a lower H/C ratio (black arrows).

While these data do not show the molecular structures present, they clearly indicate a progression of O/C ratio (Figures 1 and 2) and a change in compound classes (Figure S3) between the three fractions. This progression is consistent with increased partitioning to the aqueous phase as oxygenation increases. As oxygenation initially increases, compounds become more likely to remain in the interfacial region because of the presence of both polar and nonpolar functional groups. Further oxygenation shifts the solubility more to the aqueous fraction. Molecular structure, not just oxygen content, is an important factor in the partitioning behavior, and modeling efforts must take into account both factors that have been illustrated by these measurements and molecular analysis. Compositional classifications illustrate the chemical differences of each fraction.

Figure S3 shows the percentage of observed molecules corresponding to each of these classifications within the oil, IM, and DOM_{HC} fractions. The majority of the compounds found in the oil fraction were unsaturated low oxygen (43%) and aliphatic (48%) classes. The IM fraction had the highest percentage of unsaturated low oxygen classes (53%) and about 38% aliphatic classes. The chemical differences of oxygenated oil compounds observed for the three fractions provides an additional tool for understanding and predicting the fate and behavior of these photoproducts. The presence of unsaturated, high oxygen compounds exclusively in the aqueous phase indicates that an oxygen content threshold exists for compounds to remain in the oil or interfacial fractions.

Oxygen Partitioning is Dependent on Oxygen/Carbon Content. Although the mass spectrometry results do not identify individual structures, they do identify tens-of-thousands of elemental compositions in each step of the progression, enabling a unique opportunity to investigate the oxygen/carbon content dependence of partitioning behavior and expose the reasons behind the large O_x heteroatom class overlap (Figure 1). A plot of all identified elemental compositions in each step of the progression by O/C versus carbon number (Figure 3) reveals the tendency of lower oxygenated species to remain oil soluble over the entire carbon number range (left). A further increase in oxygen content yields interfacially active material at higher O/C ratios than the oil-soluble species but at the expense of higher carbon number species (middle). Thus, higher carbon number species require

https://dx.doi.org/10.1021/acs.energyfuels.9b04408
Energy Fuels 2020, 34, 4721−4726

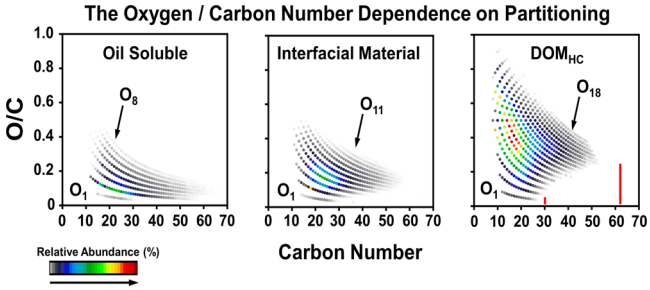

Figure 3. O/C ratio vs carbon number plots identifying elemental compositions in each step of the progression.

higher O/C ratios to become interfacially active. The trend continues and is readily apparent in the DOM_{HC} species, as the most abundant O/C ratio increases to 0.5 (also highlighted in Figure 2) but is accompanied by a narrowing of the carbon number range and exclusion of the highest carbon number species (highlighted by red lines, right). Thus, irrespective of the structure, species that contain 50 carbons require at least 14 oxygens per molecule to become water soluble, and the required oxygen decreases with decreased carbon number. Similar trends can be seen for all species presented. Finally, the reason for the large overlap in O_x heteroatom classes between the three progressions is revealed: there is a clear carbon number dependence on partitioning that is not captured by grouping transformation species by heteroatom content; it is, however, revealed by plotting the data by O/C ratio versus carbon number. These results include quantitative measures of overlapping carbon number and oxygen number dependencies that were not previously known.

All of the results discussed above are in clear agreement with equilibrium models of solubility.[33] As the carbon number of a molecule increases, it is more likely to be soluble in a hydrocarbon-like solvent (oil). As the oxygen content of a molecule increases, it is more likely to be soluble in a polar solvent (water). Molecules containing both polar and nonpolar regions in appropriate proportions will tend to be most stable as interfacial species with the nonpolar regions in the oil phase and the polar regions in the water phase. It is important to recognize that any molecule will partition among these three fractions, but the equilibrium will shift across these fractions according to the extent of polar and nonpolar functional groups in each molecule. Figure 3 illustrates that there is both O/C dependence and H/C dependence on partitioning behavior, a point, to our knowledge, that has not previously been reported. While these trends are very clear, the detailed molecular structures remain unknown. However, the results of this study provide an empirical tool for assessing the partitioning behavior of petroleum oxygenation products. For the oil used in this study, solubility shifted to the aqueous phase for molecules with an O/C ratio of greater than 0.4. For species with O/C < 0.4, the partitioning between the three phases followed clear trends based on carbon number.

Light-Initiated Changes in DOC and Optical Properties. The focus of this study was on characterizing aspects of the photo-oxygenated products across all three fractions, oil-soluble, IM, and DOM_{HC} and to provide evidence regarding the progression to DOM_{HC} during sunlight-driven transformation processes. Analysis of DOC revealed high concentrations in the DOM_{HC} fraction at 65.7 ± 4.8 mg C L^{-1} compared to the dark (3.3 mg C L^{-1}). These results are in agreement with previous studies that implicate photochemical transformation as a dominant process for production of large quantities of DOM_{HC} from petroleum.[4,27,34,35]

The contour plots of the EEMs show unique characteristics between the three fractions. Figure 4 illustrates color-contour

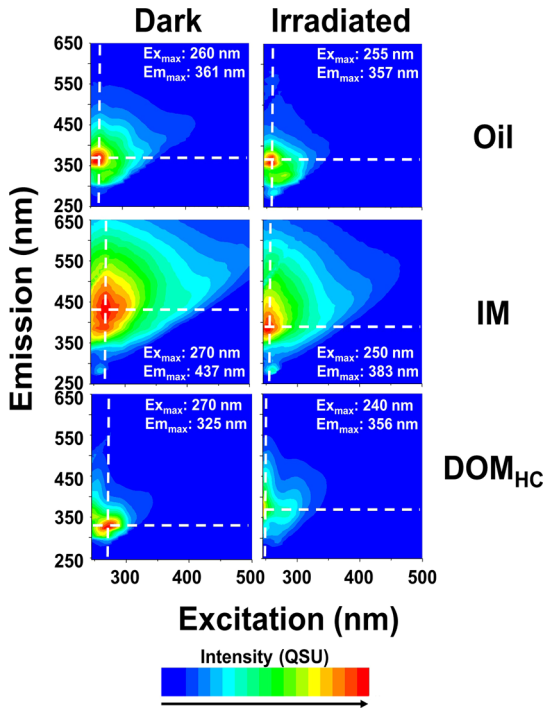

Figure 4. Color-contour plots obtained by EEM spectroscopy for the dark and irradiated oil, IM, and produced DOM_{HC}. Dotted white lines represent the maximum intensities for excitation and emission (shown in red).

plots for the oil, IM, and DOM_{HC} fractions before and after light exposure. The dotted white lines indicate the maximum excitation (Ex_{max}) and emission (Em_{max}) between the dark and light samples. The oil-soluble dark versus light fraction indicated a very slight shift to shorter wavelengths (blue shift). After irradiation, the IM fraction shifted to shorter wavelength (blue shift) with an Ex_{max} of 250 from 270 nm and an Em_{max} of 383 nm from 437 nm. We hypothesize that the blue shift in both excitation and emission indicates a loss of light-absorbing species in the IM fraction after photo-oxidation. According to Bugden et al. (2008),[10] high intensity bands observed at emission wavelengths around 340 nm are associated with 1−3 ring aromatic structures, and 3+ ring aromatics are associated with emission wavelengths of 445 nm.[36] Applying these guidelines to Figure 4, the irradiated oil contour plots likely contain 1−3 ring aromatic compounds, the IM contour plots likely comprise 3+ ring aromatics, and the DOM_{HC} has signatures of both.[10,36] The EEMs data reveal the difficulties associated with mass spectral characterization of the IM fraction and give insights into the emulsion behavior of these fractions, as stated in Clingenpeel et al. 2017.[18] For example, the IM fraction in Figure 4 shows clear evidence that the material is highly aromatic, yet the FT-ICR MS data in Figure S3 show only a small percentage of aromatics. This is why other analyses are necessary in combination with FT-ICR MS to characterize complex mixtures.

https://dx.doi.org/10.1021/acs.energyfuels.9b04408
Energy Fuels 2020, 34, 4721−4726

CONCLUSIONS

It has long been postulated that sunlight alters the biogeochemical cycling of oil entering aquatic environments. This study deepens our understanding of the mechanism of IM formation when oil is exposed to water and/or sunlight. The FT-ICR data provides empirical values that can be used to predict shifts from oil solubility to interfacial activity to aqueous solubility. Furthermore, there is a clear continuum of oxygenated compounds that contribute to the formation of each fraction after sunlight exposure which is governed by polarity. Our data corroborate with the proposed mechanism of Thingstad and Pengerud (1983), which states that "photochemical oxidation of oil components leads to the formation of surface-active, oil-soluble compounds."[12] Furthermore, we provide evidence that all of the polar compounds do not stay entrained in the oil layer. In fact, we show that the polar groups undergo transition into the IM fraction and eventually become water-soluble (DOM_{HC}) after light exposure. These data definitively show the existence of a sunlight-induced intermediate layer at the oil−water interface that to our knowledge has not previously been characterized. The formation of interfacially active compounds from oxygenation of oil is extremely important because these compounds can act as emulsifying agents or otherwise alter the exchange of reactants and nutrients at the oil−water interface. Consequently, the physical, chemical, and biological behavior of oil is impacted by the presence of the IM fraction. For the aqueous material, increased water solubility and bioavailability are imparted because of photo-oxygenation. Additional studies are needed to understand the kinetics and mechanisms of the progression of oil into IM and DOM_{HC} fractions as well as to understand the behavior of these photoproduct pools as they evolve in the environment.

ASSOCIATED CONTENT

Supporting Information

The Supporting Information is available free of charge at https://pubs.acs.org/doi/10.1021/acs.energyfuels.9b04408.

Blank EEM spectra, heteroatom oxygen class graphs, percent assigned formulas, and van Krevelen diagrams (PDF)

AUTHOR INFORMATION

Corresponding Authors

Ryan P. Rodgers − *National High Magnetic Field Laboratory, Florida State University, Tallahassee, Florida 32310-4005, United States;* orcid.org/0000-0003-1302-2850; Email: rodgers@magnet.fsu.edu

Matthew A. Tarr − *Department of Chemistry, University of New Orleans, New Orleans, Louisiana 70148, United States;* orcid.org/0000-0002-3399-1336; Email: mtarr@uno.edu

Authors

Phoebe Zito − *National High Magnetic Field Laboratory, Florida State University, Tallahassee, Florida 32310-4005, United States*

David C. Podgorski − *Pontchartrain Institute for Environmental Sciences and Department of Chemistry, University of New Orleans, New Orleans, Louisiana 70148, United States;* orcid.org/0000-0002-1070-5923

Tessa Bartges − *National High Magnetic Field Laboratory, Florida State University, Tallahassee, Florida 32310-4005, United States*

François Guillemette − *Research Center for Watershed-Aquatic Ecosystem Interactions (RIVE), Department of Environmental Sciences, Université du Québec à Trois-Rivières, Trois-Rivières, Québec G8Z 4M3, Canada*

J. Alan Roebuck, Jr. − *Southeast Environmental Research Center and Department of Chemistry and Biochemistry, Florida International University, Miami, Florida 33199, United States*

Robert G. M. Spencer − *National High Magnetic Field Laboratory and Department of Earth, Ocean and Atmospheric Science, Florida State University, Tallahassee, Florida 32310-4005, United States*

Complete contact information is available at: https://pubs.acs.org/10.1021/acs.energyfuels.9b04408

Notes

The authors declare no competing financial interest.

ACKNOWLEDGMENTS

This research was made possible in part by a grant from The Gulf of Mexico Research Initiative (R.P.R.) and in part by the National Science Foundation CHE-1507295 (M.A.T.) and DMR-1157490 (NHMFL, Tallahassee, Fl.). P.Z. was partially funded by Shell Global Solutions Inc. for manuscript preparation. Data are publicly available through the Gulf of Mexico Research Initiative Information & Data Cooperative (GRIIDC) at https://data.gulfresearchinitiative.org (doi: <10.7266/n7-bqdh-w733>). We thank Sarah Ellen Johnston for her assistance with obtaining DOC analysis and Amy Clingenpeel for performing the IM separations. F.G. was partly supported by a Fonds de Recherche du Québec—Nature et Technologies postdoctoral fellowship. The authors extend a special thanks to Rudolf Jaffé for his feedback and intellectual contribution to this study.

REFERENCES

(1) Aeppli, C.; Nelson, R. K.; Carmichael, C. A.; Arakawa, N.; Aluwihare, L. I.; Valentine, D. L.; Reddy, C. M. Characterization of recalcitrant oxygenated hydrocarbons formed upon oil weathering after the Deepwater Horizon disaster. *Abstracts of Papers of the American Chemical Society*, 2013; American Chemical Society, GEOC-150.

(2) Ward, C. P.; Sharpless, C. M.; Valentine, D. L.; French-McCay, D. P.; Aeppli, C.; White, H. K.; Rodgers, R. P.; Gosselin, K. M.; Nelson, R. K.; Reddy, C. M. Partial Photochemical Oxidation Was a Dominant Fate of Deepwater Horizon Surface Oil. *Environ. Sci. Technol.* **2018**, *52*, 1797−1805.

(3) Griffiths, M. T.; Da Campo, R.; O'Connor, P. B.; Barrow, M. P. Throwing Light on Petroleum: SImulated Exposure of Crude Oil to Sunlight and Characterization Using Atmospheric Pressure Photoionization Fourier Transform Ion Cyclotron Resonance Mass Spectrometry. *Anal. Chem.* **2014**, *86*, 527−534.

(4) Harriman, B. H.; Zito, P.; Podgorski, D. C.; Tarr, M. A.; Suflita, J. M. Impact of Photooxidation and Biodegradation on the Fate of Oil Spilled During the Deepwater Horizon Incident: Advanced Stages of Weathering. *Environ. Sci. Technol.* **2017**, *51*, 7412−7421.

(5) Bacosa, H. P.; Erdner, D. L.; Liu, Z. Differentiating the roles of photooxidation and biodegradation in the weathering of Light Louisiana Sweet crude oil in surface water from the Deepwater Horizon site. *Mar. Pollut. Bull.* **2015**, *95*, 265−272.

(6) Ray, P. Z.; Chen, H.; Podgorski, D. C.; McKenna, A. M.; Tarr, M. A. Sunlight creates oxygenated species in water-soluble fractions of Deepwater horizon oil. *J. Hazard. Mater.* **2014**, *280*, 636−643.

(7) Zhou, Z.; Liu, Z.; Guo, L. Chemical evolution of Macondo crude oil during laboratory degradation as characterized by fluorescence EEMs and hydrocarbon composition. *Mar. Pollut. Bull.* **2013**, *66*, 164−175.
(8) Zhou, Z.; Guo, L.; Shiller, A. M.; Lohrenz, S. E.; Asper, V. L.; Osburn, C. L. Characterization of oil components from the Deepwater Horizon oil spill in the Gulf of Mexico using fluorescence EEM and PARAFAC techniques. *Mar. Chem.* **2013**, *148*, 10−21.
(9) Bianchi, T. S.; Osburn, C.; Shields, M. R.; Yvon-Lewis, S.; Young, J.; Guo, L.; Zhou, Z. Deepwater Horizon Oil in Gulf of Mexico Waters after 2 Years: Transformation into the Dissolved Organic Matter Pool. *Environ. Sci. Technol.* **2014**, *48*, 9288−9297.
(10) Bugden, J. B. C.; Yeung, C. W.; Kepkay, P. E.; Lee, K. Application of ultraviolet fluorometry and excitation-emission matrix spectroscopy (EEMS) to fingerprint oil and chemically dispersed oil in seawater. *Mar. Pollut. Bull.* **2008**, *56*, 677−685.
(11) Zhou, Z.; Guo, L. Evolution of the optical properties of seawater influenced by the Deepwater Horizon oil spill in the Gulf of Mexico. *Environ. Res. Lett.* **2012**, *7*, 025301.
(12) Thingstad, T.; Pengerud, B. The formation of "chocolate mousse" from Statfjord crude oil and seawater. *Mar. Pollut. Bull.* **1983**, *14*, 214−216.
(13) Aeppli, C.; Carmichael, C. A.; Nelson, R. K.; Lemkau, K. L.; Graham, W. M.; Redmond, M. C.; Valentine, D. L.; Reddy, C. M. Oil Weathering after the Deepwater Horizon Disaster Led to the Formation of Oxygenated Residues. *Environ. Sci. Technol.* **2012**, *46*, 8799−8807.
(14) Hall, G. J.; Frysinger, G. S.; Aeppli, C.; Carmichael, C. A.; Gros, J.; Lemkau, K. L.; Nelson, R. K.; Reddy, C. M. Oxygenated weathering products of Deepwater Horizon oil come from surprising precursors. *Mar. Pollut. Bull.* **2013**, *75*, 140−149.
(15) Arey, J. S.; Nelson, R. K.; Reddy, C. M. Disentangling Oil Weathering Using GC×GC. 1. Chromatogram Analysis. *Environ. Sci. Technol.* **2007**, *41*, 5738−5746.
(16) Nicodem, D. E.; Guedes, C. L. B.; Correa, R. J. Photochemistry of petroleum. *Mar. Chem.* **1998**, *63*, 93−104.
(17) Clingenpeel, A. C.; Robbins, W. K.; Corilo, Y. E.; Rodgers, R. P. Effect of the Water Content on Silica Gel for the Isolation of Interfacial Material from Athabasca Bitumen. *Energy Fuels* **2015**, *29*, 7150−7155.
(18) Clingenpeel, A. C.; Rowland, S. M.; Corilo, Y. E.; Zito, P.; Rodgers, R. P. Fractionation of Interfacial Material Reveals a Continuum of Acidic Species That Contribute to Stable Emulsion Formation. *Energy Fuels* **2017**, *31*, 5933−5939.
(19) Schramm, L. L. *Emulsions: Fundamentals and Applications in the Petroleum Industry*; American Chemical Society: Washington, D.C., 1992; Vol. *231*.
(20) Stenson, A. C.; Marshall, A. G.; Cooper, W. T. Exact masses and chemical formulas of individual Suwannee River fulvic acids from ultrahigh resolution electrospray ionization Fourier transform ion cyclotron resonance mass spectra. *Anal. Chem.* **2003**, *75*, 1275−1284.
(21) Kujawinski, E. B.; Hatcher, P. G.; Freitas, M. A. High-resolution Fourier transform ion cyclotron resonance mass spectrometry of humic and fulvic acids: improvements and comparisons. *Anal. Chem.* **2002**, *74*, 413−419.
(22) Koch, B. P.; Dittmar, T. From mass to structure: an aromaticity index for high-resolution mass data of natural organic matter. *Rapid Commun. Mass Spectrom.* **2006**, *20*, 926−932.
(23) Fay, J. A. Physical Processes in the spread of oil on a water surface. *Int. Oil Spill Conf. Proc.* **1971**, *1971*, 463−467.
(24) King, S. M.; Leaf, P. A.; Olson, A. C.; Ray, P. Z.; Tarr, M. A. Photolytic and photocatalytic degradation of surface oil from the Deepwater Horizon spill. *Chemosphere* **2014**, *95*, 415−422.
(25) Jarvis, J. M.; Rodgers, R. P.; Robbins, W. K. Isolation of interfacial material from organic matrices. U.S. Patent 20,140,110,343 A1, April 24, 2014.
(26) Dittmar, T.; Koch, B.; Hertkorn, N.; Kattner, G. A simple and efficient method for the solid-phase extraction of dissolved organic matter (SPE-DOM) from seawater. *Limnol. Oceanogr.: Methods* **2008**, *6*, 230−235.
(27) Zito, P.; Ghannam, R.; Bekins, B. A.; Podgorski, D. C. Examining the Extraction Efficiency of Petroleum-Derived Dissolved Organic Matter in Contaminated Groundwater Plumes. *Groundwater Monit. Rem.* **2019**, *39*, 25−31.
(28) Blakney, G. T.; Hendrickson, C. L.; Marshall, A. G. Predator data station: A fast data acquisition system for advanced FT-ICR MS experiments. *Int. J. Mass Spectrom.* **2011**, *306*, 246−252.
(29) Kaiser, N. K.; Quinn, J. P.; Blakney, G. T.; Hendrickson, C. L.; Marshall, A. G. A Novel 9.4 Tesla FTICR Mass Spectrometer with Improved Sensitivity, Mass Resolution, and Mass Range. *J. Am. Soc. Mass Spectrom.* **2011**, *22*, 1343−1351.
(30) Savory, J. J.; Kaiser, N. K.; McKenna, A. M.; Xian, F.; Blakney, G. T.; Rodgers, R. P.; Hendrickson, C. L.; Marshall, A. G. Parts-Per-Billion Fourier Transform Ion Cyclotron Resonance Mass Measurement Accuracy with a "Walking" Calibration Equation. *Anal. Chem.* **2011**, *83*, 1732−1736.
(31) Corilo, Y. *EnviroOrg*; Florida State University: Tallahassee, 2015.
(32) Šantl-Temkiv, T.; Finster, K.; Dittmar, T.; Hansen, B. M.; Thyrhaug, R.; Nielsen, N. W.; Karlson, U. G. Hailstones: A Window into the Microbial and Chemical Inventory of a Storm Cloud. *PLoS One* **2013**, *8*, No. e53550.
(33) Andersen, S. I.; Speight, J. G. Thermodynamic models for asphaltene solubility and precipitation. *J. Pet. Sci. Eng.* **1999**, *22*, 53−66.
(34) Podgorski, D. C.; Zito, P.; McGuire, J. T.; Martinovic-Weigelt, D.; Cozzarelli, I. M.; Bekins, B. A.; Spencer, R. G. M. Examining Natural Attenuation and Acute Toxicity of Petroleum-Derived Dissolved Organic Matter with Optical Spectroscopy. *Environ. Sci. Technol.* **2018**, *52*, 6157−6166.
(35) Zito, P.; Podgorski, D. C.; Johnson, J.; Chen, H.; Rodgers, R. P.; Guillemette, F.; Kellerman, A. M.; Spencer, R. G. M.; Tarr, M. A. Molecular-Level Composition and Acute Toxicity of Photosolubilized Petrogenic Carbon. *Environ. Sci. Technol.* **2019**, *53*, 8235−8243.
(36) Wakeman, S. G. Synchronous Fluorescence Spectroscopy and Its Application to Indigenous and Petroleum-Derived Hydrocarbons in Lacustrine Sediments. *Environ. Sci. Technol.* **1977**, *11*, 272−276.

https://dx.doi.org/10.1021/acs.energyfuels.9b04408
Energy Fuels 2020, 34, 4721−4726